공학석사학위논문

Electrochemical and mechanical properties of $LiMn_2O_4$ according to particle morphology

입자 형상에 따른 $LiMn_2O_4$의 전기화학 및 기계적 특성

2015년 2월

서울대학교 대학원

화학생물공학부

신 소 영

Abstract

Lithium-ion battery (LIB) is currently used as a power source in mobile devices and electric vehicles. One of the requirements for those uses is high volumetric energy density and it can be realized by a step in electrode making process called pressing. Pressing can, however, damage active materials with the high pressure applied to them, and this particle breakage phenomenon can cause side effects in LIBs.

In this work, the effect of pressing on particle breakage and LIB performance is studied. Active material used in this study is spinel structured $LiMn_2O_4$. Using $LiMn_2O_4$ it was confirmed from FE-SEM image, high temperature cycle and storage performance that pressing can induce particle breakage and it can degrade cell performance.

To alleviate this problem, the relation between particle morphology and breaking property was studied. First the effect of morphology was checked in the level of particle by micro compression test. A criterion established from hard carbon system was used to interpret the results of micro compression test. As a result, spherical $LiMn_2O_4$ showed more resistance to breakage based on the criterion.

Next, the experiment was performed for electrodes. Electrodes whose active

materials are either spherical or non-spherical $LiMn_2O_4$s were compared based on FE-SEM images and high temperature storage test. The result agreed with that of micro compression test, showing that spherical $LiMn_2O_4$s are more resistant to breakage during pressing and preferable also in respect of electrode performance.

This study has found that particle breakage during pressing should be considered an important factor in LIB using $LiMn_2O_4$ as active material and morphology control can handle this problem. Micro compression test was suggested as a tool for studying mechanical properties of LIB active materials with proper criteria. It is expected that the results and methodologies used in the study can also be used for various active materials other than spinel $LiMn_2O_4$.

.....

Keywords: Lithium-ion battery, pressing, breakage, morphology, $LiMn_2O_4$

Student number 2013-22526

List of Figures

List of Tables

Contents

1. Introduction

As lithium-ion battery (LIB) is expanding its use from mobile devices to electric vehicles and energy storage systems, various requirements are needed. Among many requirements, volumetric energy density is especially becoming important considering slim devices and EVs where LIBs should exert much energy within limited space. Volumetric energy density is the product of working voltage and volumetric capacity. Change in active material can increase working voltage or energy density, but it is difficult to change active materials in the manufacturing process in a short time. The easiest way to increase volumetric energy density is to increase the degree of pressing of electrodes. The high pressure, however, can make great stress in active materials, and it can lead to particle breakage. Many studies already dealt with fracture of active materials. According to these studies, fracture affects fading of LIB causing additional electrolyte decomposition and contact loss between active materials[1, 2]. However, these studies are related to the stress caused by charge and discharge, and studies on active material fracture or breakage caused by pressing process have been limited until now. Some of the studies dealt with reorientation of particles, possibility of fracture or deformation[3, 4], but fracture and its effect haven't been investigated in detail.

In this study, first it will be confirmed that the breakage of active materials occurs by pressing, and its effect on cell performance will be investigated. To do this study, spinel

structured $LiMn_2O_4$ was used. $LiMn_2O_4$ has been suggested as an active material that can substitute $LiCoO_2$ for it is economical, environmentally benign and has stable structure during charge and discharge. The volumetric capacity of $LiMn_2O_4$, however, is lower than that of $LiCoO_2$, so the degree of pressing can be higher for $LiMn_2O_4$ to realize the same volumetric energy density as $LiCoO_2$. Moreover dissolution of manganese ion from $LiMn_2O_4$ surface is believed to be the most important reason for capacity fading of $LiMn_2O_4$ cell, so it was thought that particle breakage from pressing should be considered an important factor when using $LiMn_2O_4$.

Second, to minimize particle breakage of $LiMn_2O_4$, the effect of morphology is studied. Before it is studied for $LiMn_2O_4$, the criterion for comparing the degree of resistance against breakage under compression will be established in the level of particle. Based on this, the effect of morphology on $LiMn_2O_4$ breakage will be investigated in the scale of electrode as well as particle.

2. Background

2.1. Fundamentals of lithium-ion batteries

An electrochemical cell consists of two electrodes with different electric potentials. The difference is the driving force for a cell to exert current to the external circuit. From the next equation, the electromotive force $\mathrm{E}^{0}_{\mathrm{cell}}$ and the change in Gibbs free energy $\Delta \mathrm{G}^{0}$ can be expressed with $\mathrm{E}_{\mathrm{RHS}}$ and $\mathrm{E}_{\mathrm{LHS}}$, each meaning higher and lower standard reduction potential among two electrodes.

$$\mathrm{E}^{0}_{cell} = E^{0}_{RHS} - E^{0}_{LHS} \quad , \qquad \Delta G^{0} = -\mathrm{nF}E^{0}_{cell}$$

Batteries consisting of one or more cells are divided into primary cells which only can discharge once and secondary cells which can charge and discharge repeatedly. Composition and working principles of lithium-ion battery (LIB), a kind of secondary battery, are described in Fig. 1. In each of the positive and negative electrodes, there are active materials that can save lithium ions in their structures, and lithium ions travel between the electrodes through the electrolyte where lithium salt is dissolved. A separator which prevents formation of a short - circuit between two electrodes without blocking the movement of lithium ions is located between two electrodes. When LIB discharges, oxidation reaction occurs at negative electrode releasing lithium ions into the electrolyte and electrons to the external circuit.

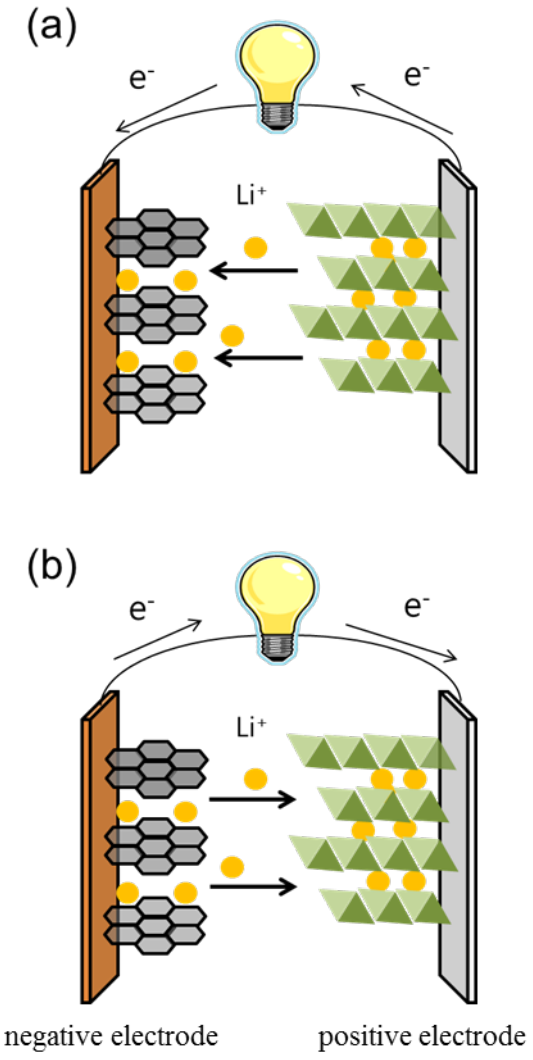

Figure 1 The components and working principle of LIB (a) charging (b) discharging

Positive electrode accepts lithium ions and electrons. The opposite phenomena occur when LIB charges and lithium ions are stored in negative electrode.

LIBs have advantages like this.

i) It shows high operation voltage as the standard reduction potentials of lithium metal or negative electrode active materials like graphite are very low. It is very preferable feature for high energy density.

ii) Manufacturing LIBs into various types of shape and size is possible which gives flexibility in designing cell system.

iii) Self discharge is less than other batteries with the formation of solid electrolyte interphase (SEI). LIB shows 5% of self-discharge per a month while 30% and 10% of the capacity loss by self-discharge is shown in Ni/MH battery and Ni/Cd battery.

iv) LIB has wide range of operation temperature. It can be used between – 20^{o}C and 60^{o}C.

2.2. Components of lithium ion batteries

2.2.1. Negative electrode materials

Negative electrode materials are preferable when they have low standard electrode potential and high specific and volumetric energy density to increase energy density. One of the best materials that fit these requirements is lithium metal. Lithium is the lightest metal having theoretical specific capacity of 3800 mA h g^{-1} and low standard electrode potential of -3.045 V *vs.* NHE (normal hydrogen electrode). However, dendrites can grow on it raising a critical safety problem, and dead lithium decreases usable capacity on repeated cycles. It is carbonaceous materials that have solved these problems. Carbonaceous materials make stable cycles possible with insertion and de-insertion of lithium ion in and out of the fixed structure and show working voltage higher than 3V having similar standard electrode voltage to lithium metal. However they have limited capacity promoting studies on alloy negative electrode materials.

2.2.1.1. Carbonaceous materials

Among several carbonaceous materials, graphite is currently used the most. It keeps its structure stable when lithium ions intercalate and de-intercalate, and the reaction occurs at potential as low as 0~0.3 V (*vs.* Li/Li^+). Lithium ions intercalate into graphite in order (stage phenomenon), and the intercalation can be represented like this.

$$xLi^+ + e + C_6 \rightarrow Li_xC_6$$

With maximum intercalation, it has structure of LiC_6 and theoretical capacity of

372 mA h g^{-1}.

Among non-graphitic carbons, there are soft carbons which are graphitized when heated over 2000℃ and hard carbons which are not. Soft carbons show higher capacity than graphite when heated under 800℃, but it shows higher discharge voltage than charge voltage giving poor energy efficiency. Hard carbons were used for initially commercialized LIBs. They show high capacity and stable cycle performance, but have disadvantages like having reactivity to moisture in the air and possibility of lithium metal deposition as it shows large capacity around 0 V[5].

2.2.1.2. Li-alloy materials

Lithium alloy materials do not let lithium ions intercalate into fixed structure, but react with them forming alloy material and returning to the original material. They have been studied a lot for they show higher capacity than graphite. Typical examples are Si and Sn. Si forms *c*-$Li_{15}Si_4$ phase with capacity of about 3580 mA h g^{-1}. Sn forms $Li_{22}Sn_5$ phase giving capacity of about 900 mA h g^{-1}[6]. However, the volume increases up to about 400% leading to damage in SEI, additional electrolyte reduction, active material fracture and thus increase in cell resistance[7]. To solve this problem, making nano-sized active materials and using nonreactive buffer materials are tried[8, 9].

2.2.2. Positive electrode materials

In many cases, positive electrode materials are transition metal oxides and provide LIB system with lithium ions. $LiCoO_2$ has been used as positive electrode material from the start of commercialization of LIB, but it has disadvantages like structural instability, toxicity of cobalt and high cost[10, 11]. Therefore oxides like $LiNiO_2$, $LiMn_2O_4$, $LiFePO_4$ have been studied for its alternatives. Oxides with Co, Ni, Mn ions at the same time were developed to get all the advantages of oxides having each of the metal ions. Although not commercialized yet, lithium-rich phase $xLi_2MnO_3 \cdot (1-x)LiMO_2$ (M=Ni, Co, Mn) is developed as a high capacity cathode material and spinel $LiNi_{0.5}Mn_{1.5}O_4$ is under study to increase energy density with its high reaction voltage[12-14].

2.2.2.1. Layered structure

In layered structure positive electrode materials, oxygen anions constitute cubic close-packed (CCP) lattice, and either transition metal ions or lithium ions exist each of the layers between anion sheets alternately. During charging, lithium ions come out of the structure increasing the repulsive force between anion sheets, and the instability of structure leads to oxygen release and phase transition. Therefore only limited capacity can be used.

$LiCoO_2$ has limits of layered structure, but is now used in many commercialized LIBs as it charges and discharges very stably within specified state-of-charge (SOC). $LiNiO_2$ can exert higher capacity than $LiCoO_2$, but is difficult to synthesize and causes cation mixing which means movement of Ni^{2+} ions into Li^+ layer[15]. $LiMnO_2$ has been studied because of its advantages in respect of cost and toxicity, but conversion to thermodynamically stable spinel structure occurs. Active materials in the form of mixed transition metal ions like $LiNi_{1-y}Mn_yCo_zO_2$ have been developed and started to be used in commercialized LIBs[16].

2.2.2.2. Spinel structure

Spinel structure is based on CCP lattice of oxygen anions just like layered structure, but has different arrays of lithium ions and transition metal ions having 3-dimensional lithium ion channel other than layered structure. The most popular example of spinel structured positive electrode material is $LiMn_2O_4$. $LiMn_2O_4$ is nontoxic, cheap and retains its structure stably during charge and discharge even at high SOC. Owing to these advantages, $LiMn_2O_4$ has long been studied as an alternative to $LiCoO_2$ and produced for commercialized LIBs. However it has a critical weak point of capacity fading during long term cycling. The first approach to this problem was done for structure. The most famous issue was Jahn-Teller distortion occurring when $LiMn_2O_4$

discharges and oxidation number of manganese ion approaches +3.5. The problem of Jahn-Teller distortion was almost solved by doping various metal ions like Li, Al, Mg, Cr[17-19] and increasing the average oxidation number of manganese ion. Despite this improvement in structural stability, $LiMn_2O_4$ still fades on repeated cycles, and the fading deteriorates in high temperature. Suggested reasons for this phenomenon include transition to more stable phase during high voltage charging, oxygen deficiency and dissolution of manganese ion. One that is getting most attention is manganese ion dissolution[20-22]. Clear explanation for how dissolved ions deteriorate LIB performance has never been suggested, but the effect on the negative electrode is believed to be much more significant than that on the positive electrode itself. Dissolved manganese ion is known to deposit on the negative electrode increasing self-discharge and electrolyte decomposition leading to capacity fading in a full cell. For positive electrode itself, increase in resistance as well as active material loss caused by dissolution of manganese ion is presented as reasons for fading[23].

$LiNi_{0.5}Mn_{1.5}O_4$ is another spinel structured positive electrode material which charges and discharges at voltages higher than 4.5 V and has possibility of being used as a material that can increase energy density in the future. However, because of this high reaction voltage, electrolyte oxidation is severe and it lowers Coulombic efficiency leading to poor cycle performance[24].

2.2.2.3. Olivine structure

The most famous example of olivine structure positive electrode material is $LiFePO_4$. Reaction voltage of $LiFePO_4$ is as low as 3.4 V *vs.* Li/Li^+, so the degree of electrolyte oxidation is low and cycle performance is very stable. However the energy density is low, and additional process like carbon coating is needed to supplement low ionic and electronic conductivity.

2.2.3. Electrolyte

2.2.3.1. Organic electrolyte

Lithium ion battery has high working voltage and cannot use aqueous electrolyte. Therefore it uses aprotic solvent with lithium salt dissolved in it. Electrolyte with high conductivity is preferable for LIBs, so the solvent should have 1) high dielectric constant to dissolve lots of lithium salt and 2) low viscosity to carry lithium ions fast. Unfortunately, there is no solvent that satisfies both of the requirements. A group of solvents like PC (propylene carbonate) or EC (ethylene carbonate) only satisfy the first requirement while DMC (dimethyl carbonate), DEC (diethyl carbonate) or EMC (Ethyl methyl carbonate) only meet the second. Therefore usually more than two solvents are mixed. For lithium salt, $LiPF_6$, $LiBF_4$, $LiClO_4$, LiBOB (lithium bis(oxalate)borate) etc.

are used and among these, $LiPF_6$ is commonly used in commercialized LIBs in that it has good properties in respect of safety, stability and ionic conductivity[25].

2.2.3.2. Polymer electrolyte

Polymer electrolyte uses polymers that can carry lithium ions, so it doesn't have the problem of leakage and has advantages in the aspects of safety and flexibility in battery design. Polymer electrolyte is expected to be used in LIBs using lithium metal as negative electrode for it is believed to decrease the chance of internal short from lithium dendrite compared to conventional system that uses organic electrolyte and porous separator. However its ionic conductivity is too low to be used in commercial LIBs. To handle this problem, gel polymer electrolyte made by immersing the polymer in organic electrolyte was suggested.

3. Experimental

3.1. Fabrication of electrode

For the charge-discharge test of $LiMn_2O_4$, two types of working electrodes were prepared. One type of the electrode was made by spreading a slurry mixture of $LiMn_2O_4$ powder (Mitsui co.), super P and poly(vinylidenefluoride) (PVdF) (94 : 3: 3 weight ratio) on a Al foil while the other was made by using the same $LiMn_2O_4$ crushed with hydraulic press. And then the slurry coated Al foils were pressed using roll presser, cut into a circle with a diameter of 1.1cm and dried at 120 for 12 h in vacuum oven.

For the electrode observation and storage test of $LiMn_2O_4$, the electrode was made by spreading a slurry mixture of $LiMn_2O_4$ powder (Mitsui co. $Li_{1.10}Mn_{1.86}Mg_{0.04}O_{3.94}$ and Nikki co. $Li_{1.08}Mn_{1.84}Al_{0.08}O_{3.96}$), super P and PVdF (90 : 5 : 5 weight ratio) on a Al foil. The slurry coated Al foils which were either roll pressed or not pressed were cut and dried in the same way as the electrodes for cycle test. The amount of slurry loaded on an electrode was about 6 mg. The electrode density of pressed and non-pressed electrode was about 2.8 g cm^{-3} and 1.5 g cm^{-3} each.

3.2. Fabrication of coin-type cell

Two-electrode 2032-type cells were assembled in Ar-filled glove box with lithium foil as a counter electrode. Used electrolyte was 1.0 *M* $LiPF_6$ in EC : EMC (3 : 7 in *vol. %*). The separator was porous PP(polypropylene)/PE(polyethylene)/PP film.

3.3. Charge-discharge cycling test

The charge-discharge cycling was conducted at high temperature (60℃) within a voltage range of 3.0 V ~ 4.3 V (*vs.* Li/Li^+) using WonATech battery cycler (WBCS-3000). For the charging, constant current of 0.5 *C* was applied until the cell voltage reaches 4.3 V (CC step), and the voltage was maintained until current drops as low as 0.1 *C* (CV step). Discharge was made by applying constant current of 0.5 *C* without CV step.

Before cycling at high temperature, the cell was cycled three times at room temperature (25℃) within a voltage range of 3.0 V ~ 4.3 V (*vs.* Li/Li^+) using WonATech battery cycler (WBCS-3000). The charging had CC and CV step and discharging had only CC step just like cycling at high temperature. The constant current for CC step was 0.1 *C*, and the CV cut-off current was 0.02 *C*.

3.4. Electrode storage test

Each of the electrodes described in 3.1 was immersed in 20 ml of electrolyte 1.0 *M* $LiPF_6$ in EC : EMC (3 : 7 in *vol. %*) in a Nalgene bottle. To block $LiMn_2O_4$ particles from coming away into the electrolyte, an electrode was inserted in a pocket made of PP-PE-PP separator, and both the electrode and the pocket were put into the Nalgene bottle. (Fig. 2) The Nalgene bottle with an electrode in it was stored at 60℃ oven for either 7, 14 or 28 days.

After the storage, the electrodes were picked out of the Nalgene bottle, and remaining electrolyte was used for inductively coupled plasma-atomic emission spectroscopy (ICP-AES, OPTIMA 4300DV, Perkin-Elmer) to measure the concentration of dissolved manganese ion.

3.5. Synthesis of hard carbon

In this study, hard carbon was used as an ideal model that can verify hypothesis, not as an LIB active material. Spherical and non-spherical hard carbons were used and for spherical hard carbons, three different carbonization temperatures were adopted.

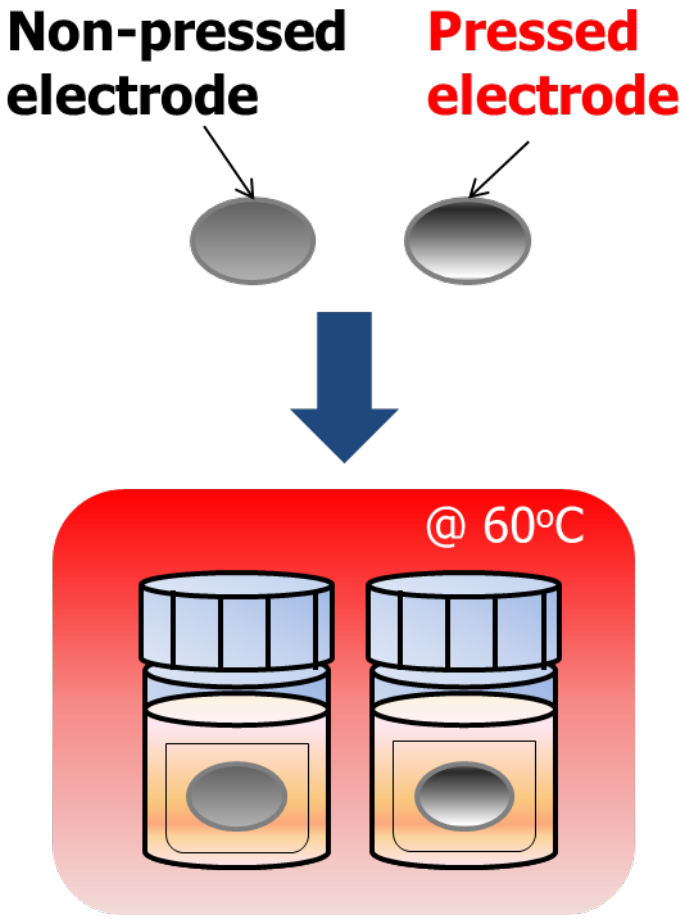

Figure 2 Storage of pressed and non-pressed electrodes in electrolyte at high temperature

3.5.1. Synthesis of spherical hard carbon

The precursor was phenolic resin from Kangnam Chemical co. First, phenolic resin was mixed with 5 *wt%* of CAB-O-SIL® TS-720 fumed silica. The mixture was heat-treated under an argon atmosphere from 25℃ to 1000℃, 800℃ or 600℃ with a heating rate of 10 min^{-1}. In the middle of the process, there was 1h of heat treating at 450℃, and additional heat treating at 1000℃, 800℃ or 600℃ was performed.[26].

After the heat treatment, fumed silica was removed using aqueous hydrofluoric acid, and then finally spherical hard carbon S-HC1000, S-HC800 and S-HC600 each carbonized at 1000℃, 800℃, 600℃ were obtained after washing and drying for overnight in vacuum oven.

3.5.2. Synthesis of non-spherical hard carbon

Non-spherical hard carbon (N-HC1000) was made from the same phenolic resin used for spherical hard carbon. Heating phenolic resin without any treatment would make the particles cluster together as the resin gets viscous when the temperature of furnace surpasses the glass transition temperature of the resin. In this study it is preferable to maintain similar size distribution of non-spherical hard carbon to that of spherical one. Therefore sodium dodecyl sulfate (SDS), a kind of surfactant, was used.

There are two steps of heat treatment in this method. First, the mixture of phenolic resin and SDS (1:1 in *wt%*) was heat-treated under an argon atmosphere from 25℃ to 170℃ with the heating rate of 10/min. In the middle of the process there was 1h of heat treating at 100℃, and additional 1h of heat treating at 170℃ was practiced. After the first step of heat treatment, SDS was removed by leaching and drying. The acquired sample was heat-treated under an argon atmosphere from 25℃ to 1000℃ with a heating rate of 10 min^{-1}. In the middle of the process there was 1h of heat treating at 450℃, and additional heat treating at 1000℃ was performed just like S-HC1000.

3.6. Micro compression test

In this study, to investigate on the breakage of particles, micro compression test was performed using MCT-W500-E micro compression testing machine (SHIMADZU co.) of Korea Electronics Technology Institute. (Fig. 3) A little amount of powder to be tested is dispersed on lower compression plate, and the plate is loaded to the testing machine. The machine applies increasing force onto each of the particles to measure the force applied to the particles at the moment of breakage, namely break force. Maximum force was 800 mN and load speed was 20.7411 mN/sec for the test on hard carbon while 200 mN and 3.8736 mN/sec for $LiMn_2O_4$.

Figure 3 Micro compression test machine (MCT-W500-E)

3.7. Other instrument and analysis method

To observe the particle morphology of powder samples and electrodes, FE-SEM (field-emission scanning electron microscopy, JEOL JSM-6700F) was used. For the observation of the electrode cross-section, cross-section polisher (JEOL, SM-09010) was used. It is the device that can cut a specimen with Ar ion beam. The cutting condition was 5kV, 0.1mA.

4. Results and discussions

4.1. Effect of electrode pressing on $LiMn_2O_4$ electrode

4.1.1. Confirmation of particle breakage induced by pressing

As mentioned in the introduction, pressing process can damage active material in the electrode. In this part, it is confirmed that $LiMn_2O_4$ particles can be crushed after pressing by comparing FE-SEM images of pressed and non-pressed electrode.

Fig. 4 is a FE-SEM image of the $LiMn_2O_4$ powder (Mitsui co.) used in this part. It shows the powder contains various micron-sized octahedrons which are clustered together.

Fig. 5 is the surface image of non-pressed and pressed electrode made of $LiMn_2O_4$ shown in Fig.4. The images show that the active material in non-pressed electrode retains its octahedral shape without any damage (Fig. 5(a)), while LMO particles in pressed electrode are broken exposing additional surface (Fig. 5(b)). Therefore, it is possible to conclude that pressing can induce breakage of $LiMn_2O_4$ particles, and the effect of breakage will be investigated in next parts.

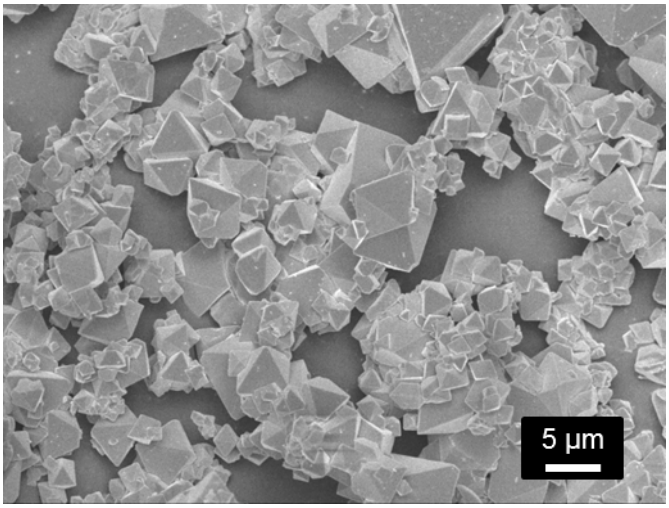

Figure 4 FE-SEM image of $LiMn_2O_4$ (Mitsui co.)

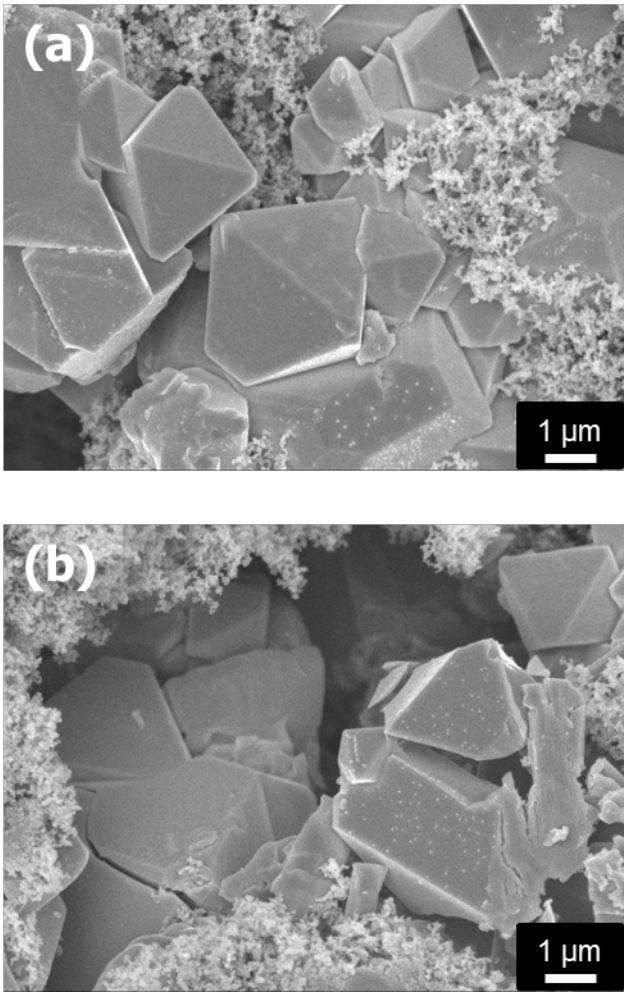

Figure 5 FE-SEM images of $LiMn_2O_4$ electrode (a) non-pressed electrode (b) pressed electrode

4.1.2. Effect of particle breakage on electrochemical properties at high temperature

To Study the effect of particle breakage on electrochemical property of $LiMn_2O_4$ electrode, charge-discharge experiment was performed. As it is believed that performance of $LiMn_2O_4$ degrades faster especially at high temperature, the cell was charged and discharged at 60℃. The electrochemical experiment was performed using two electrodes with the same degree of pressing, one made of bare $LiMn_2O_4$ powder, the other made of $LiMn_2O_4$ powder crushed by using hydraulic press. Fig.6 compares images of bare and crushed sample. Comparing pressed to non-pressed electrode was not thought to be proper to find out the effect of particle breakage in that pressing can have other effects such as improving contact between active material, conducting agent and current collector thus decreasing cell resistance.

Fig.7 shows cycle data using electrodes described just before. The most distinct feature is that Coulombic efficiency of the electrode using crushed sample is lower than the other especially during initial several cycles. From this result, particle breakage proved to worsen fading of LIB using $LiMn_2O_4$ electrode.

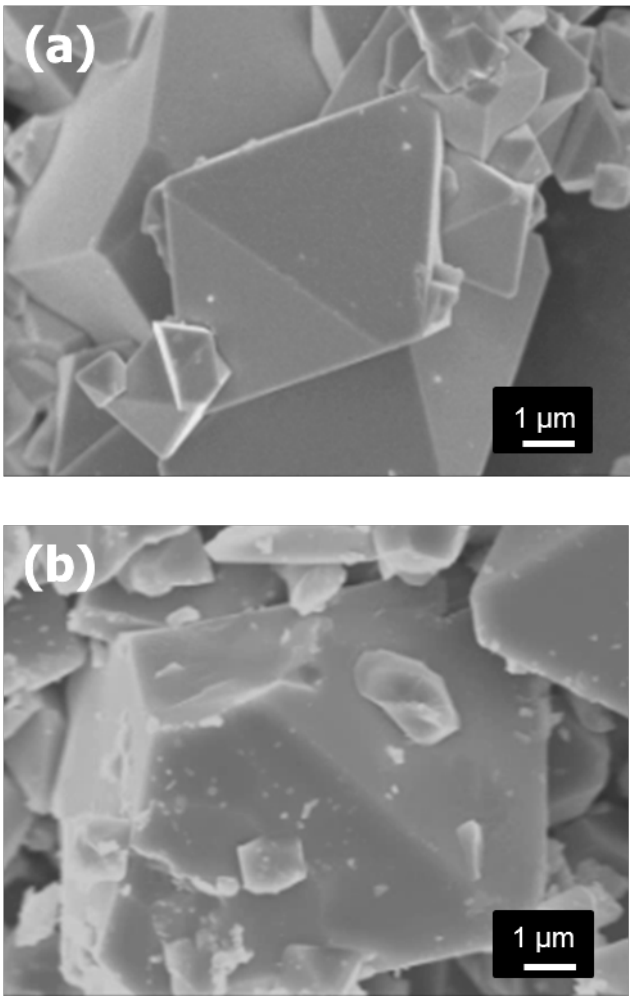

Figure 6 FE-SEM images of $LiMn_2O_4$ power used in cycling test (a) bare powder (b) crushed powder

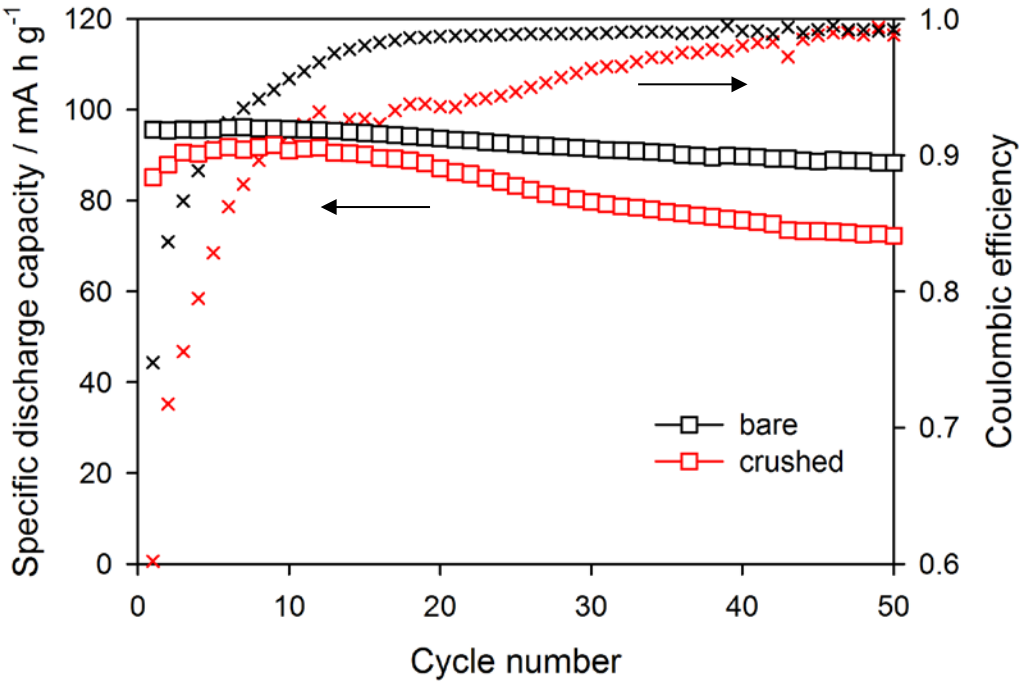

Figure 7 High temperature cycle performance of bare and crushed $LiMn_2O_4$ electrodes

One reason for this difference is thought to be increase in surface area after crushing of $LiMn_2O_4$ particles. It is well known that electrolyte decomposition occurs at the surface of active material[27, 28], and increased surface area can promote electrolyte oxidation or reduction. The newly exposed surface recognized in 4.1.1 is expected to cause additional electrolyte oxidation reducing Coulombic efficiency. Another plausible reason is the difference in the degree of stability each plane of spinel crystal has. According to M. Hirayama et al, (110) plane shows lower stability than (111) plane with thicker solid electrolyte interphase (SEI) on it[29]. As the surface of LMO particles with octahedral shape is (111) plane[30], breakage of LMO particle will expose surfaces of other direction and it will possibly change the degree of electrolyte decomposition compared to the same area of (111) plane.

4.1.3. Effect of particle breakage on manganese dissolution after storage at high temperature

Capacity fading of $LiMn_2O_4$ is believed to be related to manganese dissolution in many cases. Dissolved manganese ion can deteriorate $LiMn_2O_4$ electrode, but the most significant effect is on graphite anode on which the dissolved manganese ion deposits resulting in self discharge, thick SEI and increased resistance of the cell[31, 32]. Therefore the degree of manganese dissolution is a very important factor affecting the performance of full cell using $LiMn_2O_4$ and graphite as positive and negative electrode

active materials each. In other words, it is likely that the more manganese ion dissolves into the electrolyte, the more fading of performance occurs.

Based on this, concentration of dissolved manganese ion was measured after high temperature storage. The result is shown in table 1. More manganese ion was dissolved from pressed electrode for 14 days and 28 days storage. Just like decreased Coulombic efficiency in 4.1.2, increase in surface area and difference in plane stability is thought to have affected this result.

4.2. Establishing criterion for breaking property under compression

From the cycle test and storage experiment of 4.1, $LiMn_2O_4$ particle breakage from pressing turned out to have harmful effect on LIB. As a result, effort to minimize particle breakage is needed as pressing cannot be excluded from LIB making process. In this study, breakage of $LiMn_2O_4$ particle is investigated in respect of particle morphology. Currently commercialized $LiMn_2O_4$ products have different morphology and the difference in morphology was suspected to affect breaking property of $LiMn_2O_4$.

Table 1 Concentration of dissolved manganese ion in ppm unit after high temperature storage

Storage time	Non-pressed electrode	Pressed electrode
7 days	13	13
14 days	33	47
28 days	102	174

To handle this task, first the investigation into particle compression is made by micro compression test, and the necessity of criterion naturally comes to the fore that can be used to decide which morphology of $LiMn_2O_4$ particle is more resistant to breakage under compression. From now on, the criterion which will be used to interpret the data of micro compression test is decided and verified if it fits to particles of LIB active material whose sizes are usually in micro scale.

4.2.1 Suggestion of the criterion for breaking property

To decide which morphology of $LiMn_2O_4$ is more resistant to breakage under compression, a criterion is needed. In this study the criterion was chosen using the equation like this.

$$F_0 = \alpha S_t D^2$$

F_0 is the force applied to the particle at the moment of breakage(mN), D is particle size(μm), S_t is tensile strength(MPa) namely, maximum stress occurring at the center of particle and α is a constant according to loading type and morphology of particle[33, 34]. In this equation the product of α and S_t was chosen as the criterion on the resistance against breakage under compression as it tells how much force is needed to break the particle without considering the effect of size. As a result, the slope obtained from F_0 vs. D^2 plot will show the degree of resistance against breakage.

From now on, this criterion is verified if it fits to particles of LIB active material whose sizes are usually micro scale. To verify this criterion, a system with controlled variables was needed, and hard carbon which is easy to control morphology and hardness was selected. Using hard carbon, the criterion was verified for several cases.

4.2.2 Verification of the criterion for constant α and St

For the first step of verifying the criterion, hard carbon system with constant α and S_t was used. In other words, spherical hard carbon particles carbonized at the same temperature of 1000℃ were used for micro compression test. The synthesis method is represented in 3.2.1 and the image of synthesized hard carbon is shown in Fig. 8. The result of micro compression test is shown in Fig. 9. Each dot shows the result of micro compression test practiced on individual particles and the dashed trend line was drawn using linear regression analysis with constraint of zero y-intercept. The trend line well fitted to the micro compression test data with $R^2 = 0.9758$, so it can be clearly told that the equation we are to use reflects breaking property of the model system.

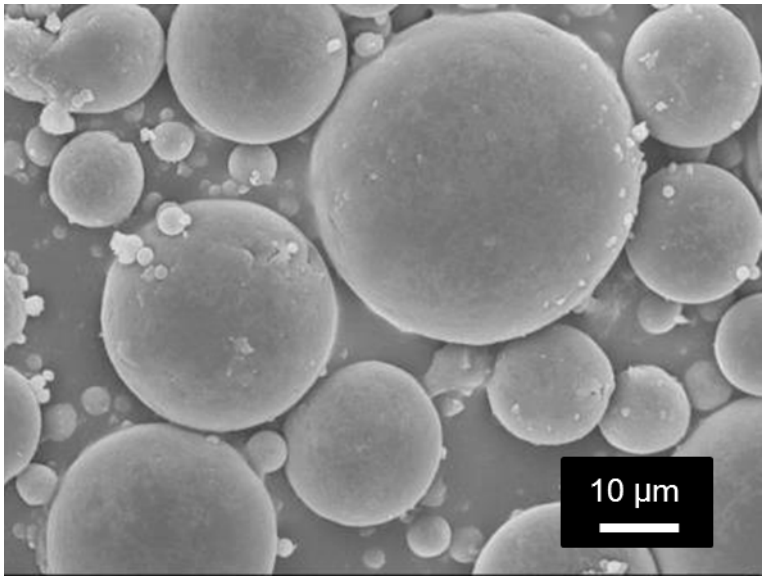

Figure 8 FE-SEM image of spherical hard carbon carbonized at 1000℃ (S-HC1000)

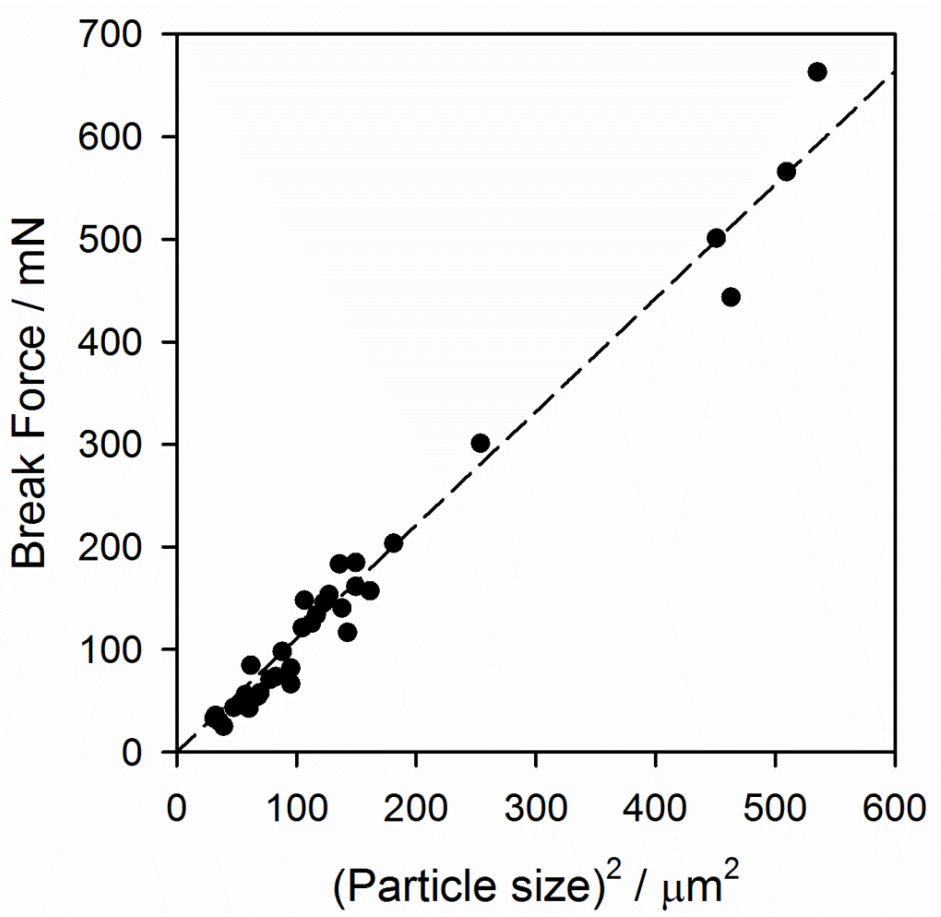

Figure 9 Result of micro compression test for spherical hard carbon carbonized at 1000℃ (S-HC1000)

4.2.3 Verification of the criterion for different values of St

For the second step of verifying the criterion, hard carbon systems with constant α and different values of S_t were compared. As the value of S_t is expected to change according to carbonization temperature, spherical hard carbons carbonized at 600℃, 800℃, 1000℃ (named as S-HC600, S-HC800, S-HC1000 each) were used for micro compression test. All the three samples showed spherical morphology as shown in Fig.10. Fig.11 shows the result where the data for S-HC600 and S-HC800 were added to Fig. 9. The dashed trend line well fitted also to the data for S-HC600 and S-HC800 with $R^2 = 0.9033, 0.8326$ each. From this result, one can conclude that the suggested equation can be applied to different values of S_t, and therefore by comparing the slopes of trend lines one another, S-HC1000 is the most and S-HC600 is the least resistant to breakage from compression. Using the slope of trend line as the criterion is thought to be valid in this case.

4.2.4 Verification of the criterion for different values of α

For the last step of verifying the criterion, hard carbon systems with different values of α and constant S_t were compared. The difference in α was made by

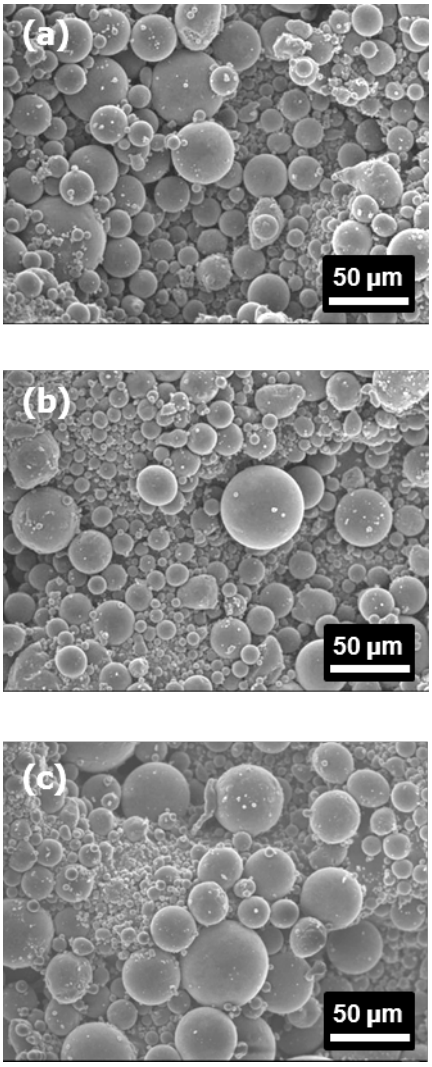

Figure 10 FE-SEM images of spherical hard carbons carbonized at (a) 1000℃ (S-HC1000), (b) 800℃ (S-HC800), (c) 600℃ (S-HC600)

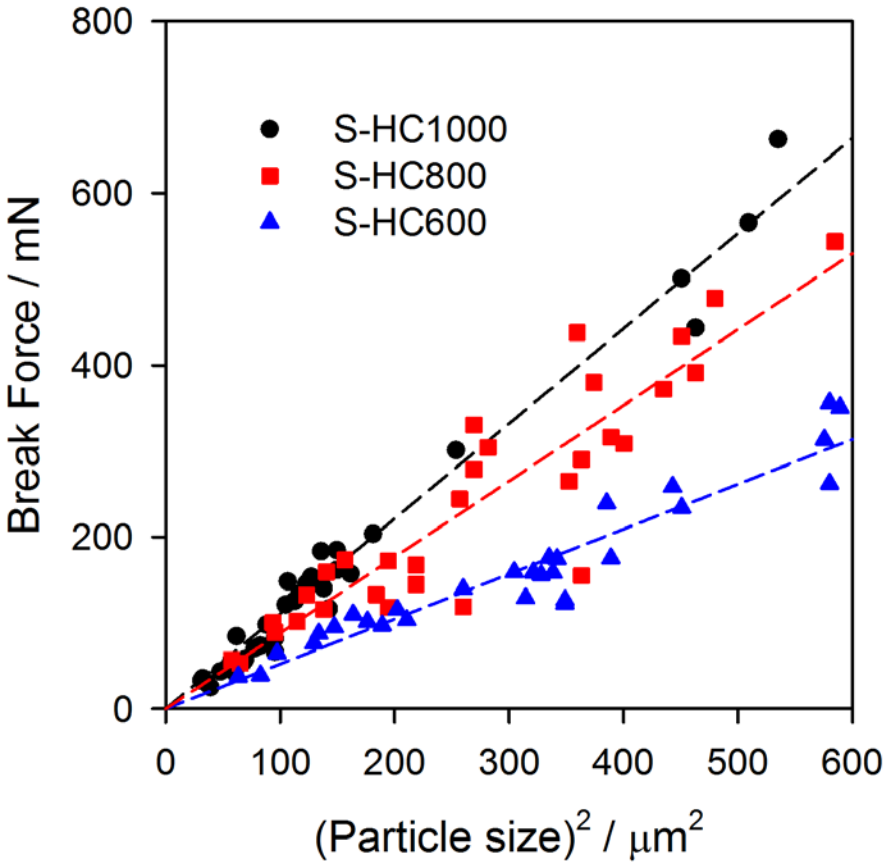

Figure 11 Result of micro compression test for hard carbons with different carbonization temperature

adopting non-spherical hard carbon (N-HC1000) whose morphology is shown in Fig.12. As N-HC1000 was made from phenolic resin with carbonization temperature of 1000℃, its S_t is thought to be the same as S-HC1000.

Fig.13 shows the micro compression test result of S-HC1000 and N-HC1000. The trend line somewhat deviates from the data of N-HC1000 with $R^2 = 0.3441$. The deviation is natural because particles of N-HC1000 don't have the same value of α. As the morphology is not spherical, α can change depending on the direction of force applied to each of the particles. D. Golchert et al. also told about the change in the resistance against breakage according to the direction of force[35]. Moreover, morphology of N-HC1000 wasn't strictly controlled, so it could also affect the quite large deviation. The slope of the trend line, however, still has significance in that the trend line approximately fits the data and the slope is the figure that can represent the breaking property of different states of particles thus serving as an average. Therefore it is possible to study on the effect of morphology by comparing the slopes of the trend lines. According to Fig. 13, spherical hard carbon shows higher value of slope and greater resistance against breakage.

From all these steps of verification, it is valid to use the slope in F_0 vs. D^2 plot as a criterion for the degree of resistance against breakage under compression.

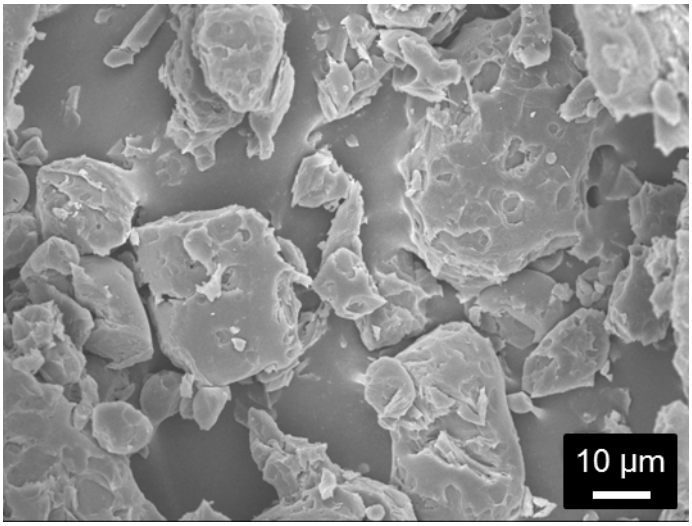

Figure 12 FE-SEM image of non-spherical hard carbon carbonized at 1000℃ (N-HC1000)

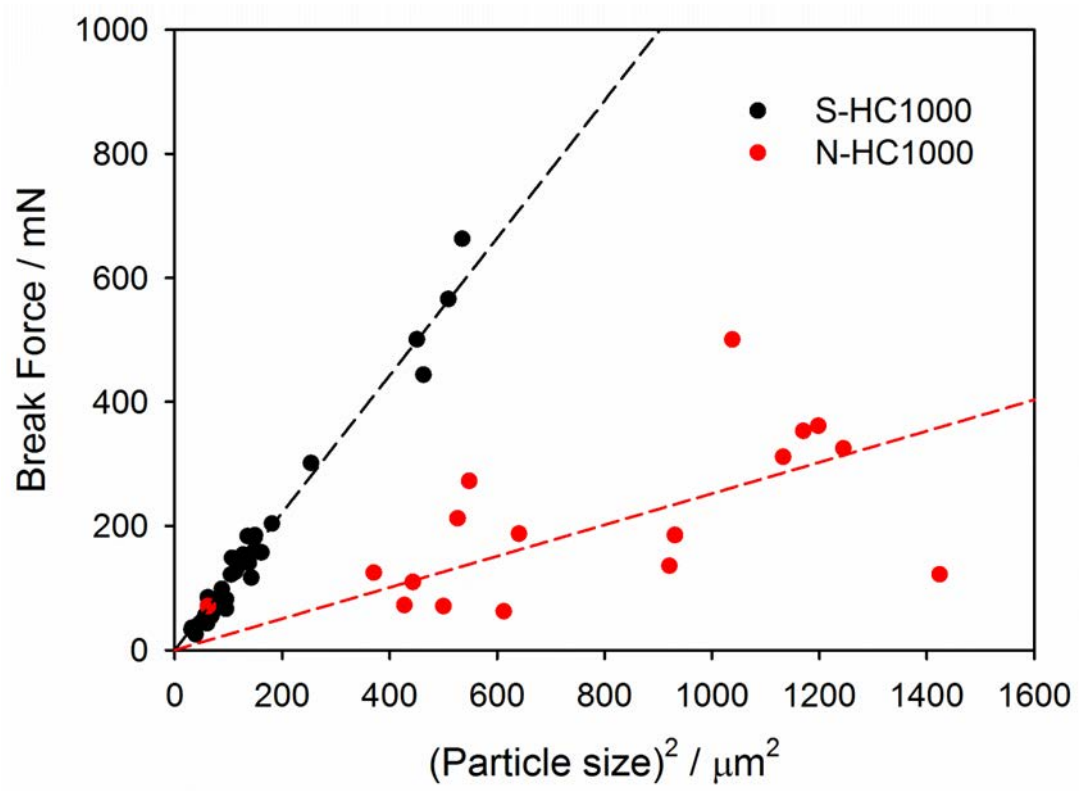

Figure 13 Result of micro compression test for spherical and non-spherical hard carbon (S-HC1000 and N-HC1000)

4.3. Effect of morphology on breakage of $LiMn_2O_4$ particle under compression

In this part, the investigation into the effect of morphology on breakage of $LiMn_2O_4$ particle is made using the verified criterion, followed by extra experiment in the level of electrode to find if the property of particle accords with the result of electrode. To perform these experiments, two kinds of commercial $LiMn_2O_4$ products with different morphologies were used, and their particle images are shown in Fig.14. The image (a) in Fig.14 shows $LiMn_2O_4$ particles of almost spherical shape (S-LMO) while (b) shows particles of irregular shape consisting of octahedrons just described in 4.1.1(N-LMO).

4.3.1. Micro compression test on $LiMn_2O_4$ particles according to its morphology

Micro compression test was performed for S-LMO and N-LMO, and the result is shown in Fig. 15. The slope of trend line for S-LMO is greater than that of N-LMO. Using the criterion we established in 4.2, we can conclude that S-LMO with spherical shape is more resistant to breakage from compression than non-spherical N-LMO, which is the same tendency as in the hard carbon model system. It is believed that

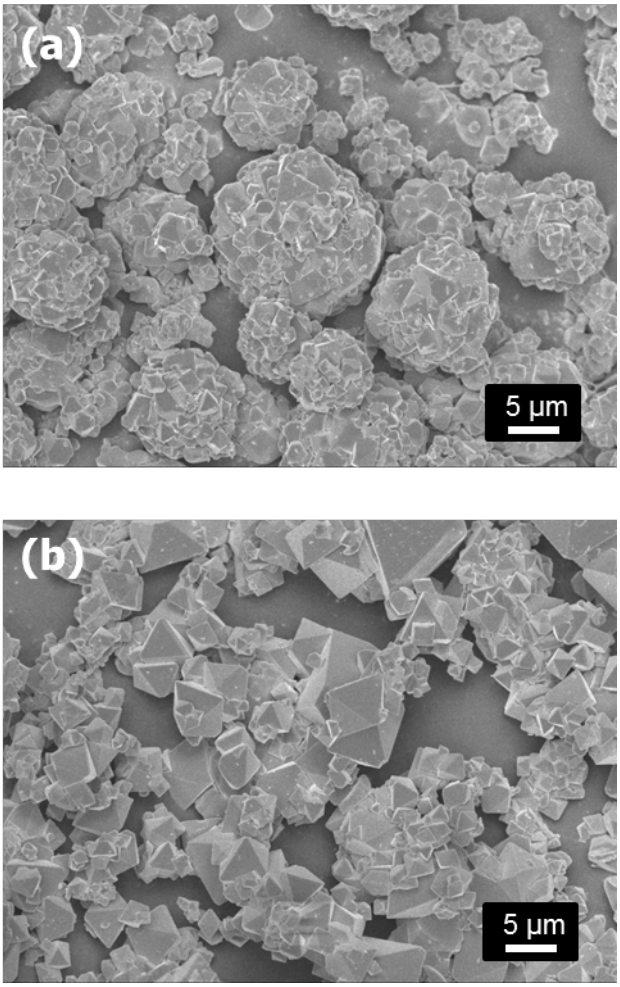

Figure 14 FE-SEM images of $LiMn_2O_4$ with different morphologies (a) spherical morphology (S-LMO, Nikki co.) (b) non-spherical morphology (N-LMO, Mitsui co.)

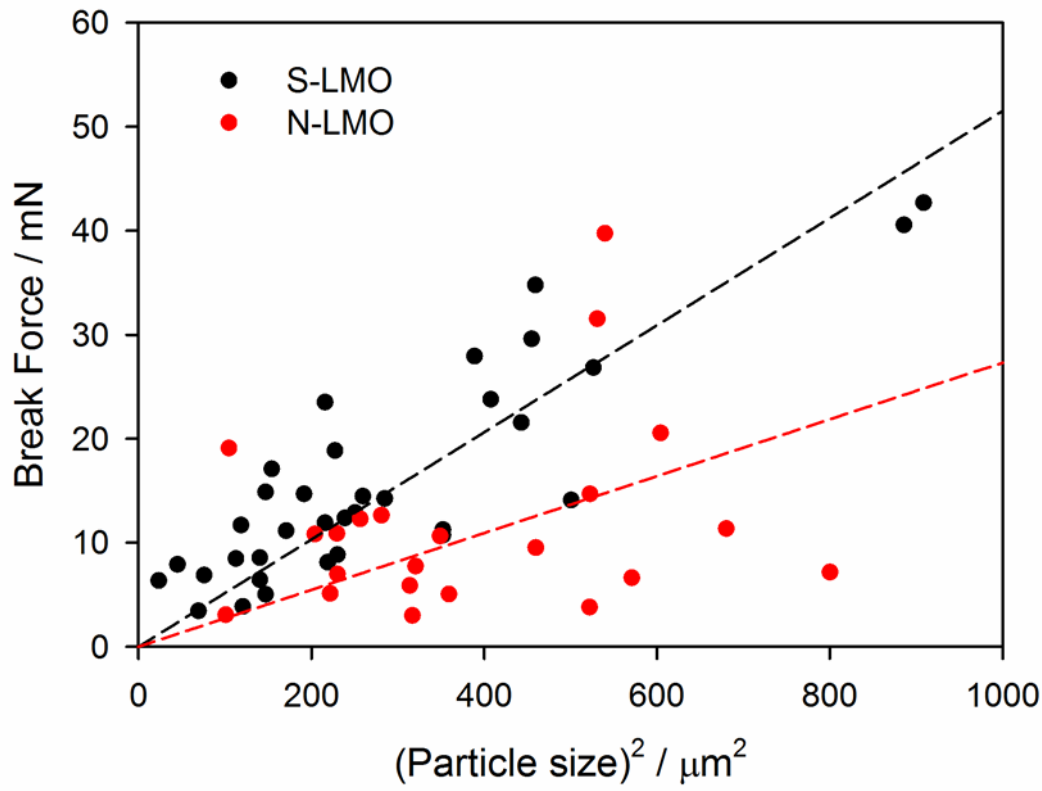

Figure 15 Result of micro compression test for spherical and non-spherical hard carbon (S-LMO and N-LMO)

spherical form is resistant to compressive breakage as it can effectively form a channel of force from one point where the force is applied to the other[35] and this seems to be applicable to LIB active materials.

4.3.2. Effect of morphology on breakage of $LiMn_2O_4$ particles in electrode

In 4.3.1, it was confirmed that $LiMn_2O_4$ particle with spherical shape is more resistant to breakage under compression. In this part, it is checked if the information obtained in the level of particle still applies to electrodes.

First, the images of cross section of $LiMn_2O_4$ electrodes were observed (Fig.16). The image (a) in Fig. 16 shows cross section of pressed electrode made of spherical S-LMO while the image (b) shows that of non-spherical N-LMO. Breakage of $LiMn_2O_4$ particle and cracks were observed in the electrode of N-LMO. In the electrode of S-LMO, however, there was little damage on $LiMn_2O_4$ particles which accords with the result of micro compression test in 4.3.1. It can be said that particles with spherical shape are more resistant to compressive breakage and it also affects the degree of particle breakage in electrodes.

Next, to confirm if the difference in the degree of particle breakage can be related to the electrode performance, storage test was done for S-LMO and N-LMO electrodes.

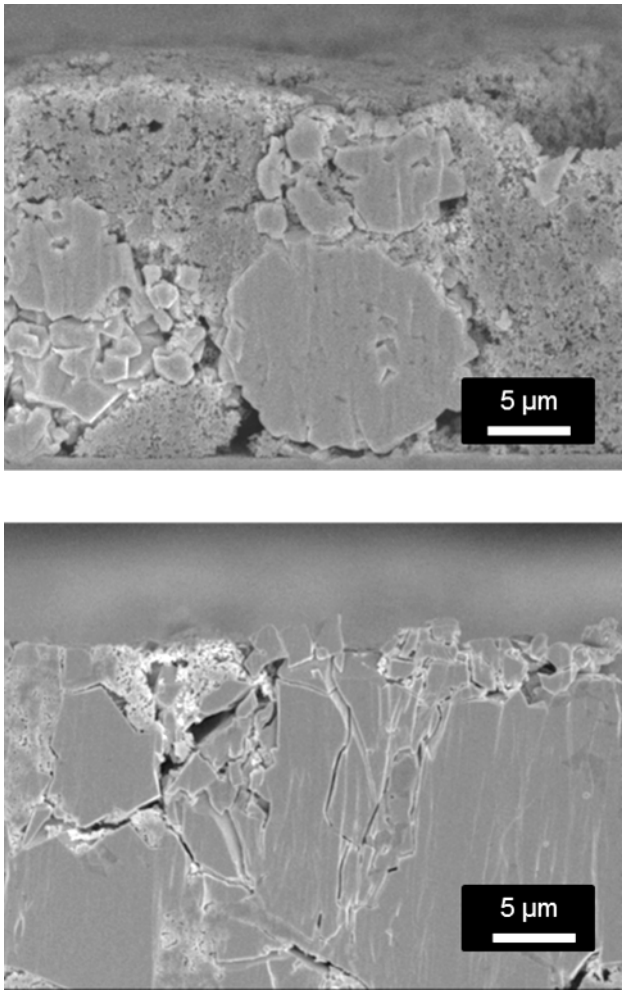

Figure 16 Cross section images of electrodes (a) spherical $LiMn_2O_4$ (S-LMO) (b) non-spherical $LiMn_2O_4$ (N-LMO)

Four types of electrodes - pressed and non-pressed S-LMO electrodes and N-LMO electrodes - were stored as described in 3.4. To study on the effect of particle breakage, the increasing ratio in the concentration of dissolved manganese ion from pressed electrode compared to that of non-pressed electrode was calculated for both $LiMn_2O_4$ electrodes.

Table 2 shows the result. The increase in manganese dissolution from pressed electrodes compared to non-pressed ones is thought to originate from the breakage of particles in pressed electrodes which can lead to exposure of new surface and following side effects described in 4.1. Therefore, the bigger increasing ratio of N-LMO means N-LMO particles are more vulnerable to breakage induced by pressing than S-LMO. Considering the micro compression test data, the difference in the degree of breakage came from the difference in the particle resistance against compressive breakage.

With all the data of this part, one can say that morphology of $LiMn_2O_4$ can affect the degree of breakage during pressing process with spherical one being preferable in this aspect. Moreover the difference in particle breakage was shown to affect the property of a cell using $LiMn_2O_4$ as active material for the amount of dissolved manganese ion during storage test is a critical factor to cell performance as explained in 4.1.3.

Table 2 Concentration of dissolved manganese ion and increasing ratio for spherical and non-spherical $LiMn_2O_4$ (S-LMO and N-LMO)

Sample	Non-pressed electrode	Pressed electrode	Increasing ratio
S-LMO	59 ppm	93 ppm	58 %
N-LMO	102 ppm	174 ppm	71 %

5. Conclusions

In this work, the effect of particle breakage during pressing was investigated, and the effect of $LiMn_2O_4$ morphology on particle breakage was studied. The results are summarized below.

(i) Particle breakage of $LiMn_2O_4$ particles can lead to critical side effects of increasing electrolyte decomposition and manganese dissolution. It was proved from high temperature cycle and storage test.

(ii) Through micro compression test, spherical $LiMn_2O_4$ was found to be more resistant to breakage under compression. In the interpretation of the test result, the slope of F_0 vs. D^2 plot was used as the criterion which was verified in hard carbon system.

(iii) The results of experiments of electrodes corresponded with micro compression test data. In other words, less number of spherical $LiMn_2O_4$ particles broke during pressing than non-spherical LMO, and it affected the electrode performance, with S-LMO showing less manganese dissolution.

This study dealt with a problem of $LiMn_2O_4$ particle breakage that can occur during pressing process, and control of $LiMn_2O_4$ morphology proved to be effective to alleviate the problem. It is thought that this result can be applied to electrodes using other active materials and be used to improve performance of commercialized cell.

References

[1] Y. Itou, Y. Ukyo, *J Power Sources*, **146**, 39-44 (2005).

[2] K. Dokko, M. Nishizawa, S. Horikoshi, T. Itoh, M. Mohamedi, I. Uchida, *Electrochem Solid St*, **3**, 125-127 (2000).

[3] J.S. Gnanaraj, Y.S. Cohen, M.D. Levi, D. Aurbach, *Journal of Electroanalytical Chemistry*, **516**, 89-102 (2001).

[4] S.G. Lee, D.H. Jeon, *J Power Sources*, **265**, 363-369 (2014).

[5] S. Flandrois, B. Simon, *Carbon*, **37**, 165-180 (1999).

[6] J.Y. Kwon, J.H. Ryu, S.M. Oh, *Electrochim Acta*, **55**, 8051-8055 (2010).

[7] J.H. Ryu, J.W. Kim, Y.E. Sung, S.M. Oh, *Electrochem Solid St*, **7**, A306-A309 (2004).

[8] T. Song, J.L. Xia, J.H. Lee, D.H. Lee, M.S. Kwon, J.M. Choi, J. Wu, S.K. Doo, H. Chang, W. Il Park, D.S. Zang, H. Kim, Y.G. Huang, K.C. Hwang, J.A. Rogers, U. Paik, *Nano Lett*, **10**, 1710-1716 (2010).

[9] M.H. Park, M.G. Kim, J. Joo, K. Kim, J. Kim, S. Ahn, Y. Cui, J. Cho, *Nano Lett*, **9**, 3844-3847 (2009).

[10] J.N. Reimers, J.R. Dahn, *J Electrochem Soc*, **139**, 2091-2097 (1992).

[11] K. Mizushima, P.C. Jones, P.J. Wiseman, J.B. Goodenough, *Materials Research Bulletin*, **15**, 783-789 (1980).

[12] Y. Talyosef, B. Markovsky, R. Lavi, G. Salitra, D. Aurbach, D. Kovacheva, M. Gorova, E. Zhecheva, R. Stoyanova, *J Electrochem Soc*, **154**, A682-A691 (2007).

[13] A.R. Armstrong, P.G. Bruce, *Electrochem Solid St*, **7**, A1-A4 (2004).

[14] T. Yoon, D. Kim, K.H. Park, H. Park, S. Jurng, J. Jang, J.H. Ryu, J.J. Kim, S.M. Oh, *J Electrochem Soc*, **161**, A519-A523 (2014).

[15] J. Vetter, P. Novak, M.R. Wagner, C. Veit, K.C. Moller, J.O. Besenhard, M. Winter, M. Wohlfahrt-Mehrens, C. Vogler, A. Hammouche, *J Power Sources*, **147**, 269-281 (2005).

[16] C.J. Han, J.H. Yoon, W. Cho, H. Jang, *J Power Sources*, **136**, 132-138 (2004).

[17] M. Yoshio, Y.Y. Xia, N. Kumada, S.H. Ma, *J Power Sources*, **101**, 79-85 (2001).
[18] Y. Gao, J.N. Reimers, J.R. Dahn, *Phys Rev B*, **54**, 3878-3883 (1996).
[19] M. Wakihara, G.H. Li, H. Ikuta, T. Uchida, *Solid State Ionics*, **86-8**, 907-909 (1996).
[20] R. Benedek, M.M. Thackeray, *Electrochem Solid St*, **9**, A265-A267 (2006).
[21] D.H. Jang, Y.J. Shin, S.M. Oh, *J Electrochem Soc*, **143**, 2204-2211 (1996).
[22] E. Iwata, K. Takahashi, K. Maeda, T. Mouri, *J Power Sources*, **81**, 430-433 (1999).
[23] D. Kim, S. Park, O.B. Chae, J.H. Ryu, Y.U. Kim, R.Z. Yin, S.M. Oh, *J Electrochem Soc*, **159**, A193-A197 (2012).
[24] T. Yoon, S. Park, J. Mun, J.H. Ryu, W. Choi, Y.S. Kang, J.H. Park, S.M. Oh, *J Power Sources*, **215**, 312-316 (2012).
[25] S.S. Zhang, *J Power Sources*, **162**, 1379-1394 (2006).
[26] O.J. Kwon, Y.S. Jung, J.H. Kim, S.M. Oh, *J Power Sources*, **125**, 221-227 (2004).
[27] C.S. Wang, A.J. Appleby, F.E. Little, *Journal of Electroanalytical Chemistry*, **519**, 9-17 (2002).
[28] M. Yoshio, H.Y. Wang, K. Fukuda, Y. Hara, Y. Adachi, *J Electrochem Soc*, **147**, 1245-1250 (2000).
[29] M. Hirayama, H. Ido, K. Kim, W. Cho, K. Tamura, J.i. Mizuki, R. Kanno, *J Am Chem Soc*, **132**, 15268-15276 (2010).
[30] J.S. Kim, K. Kim, W. Cho, W.H. Shin, R. Kanno, J.W. Choi, *Nano Lett*, **12**, 6358-6365 (2012).
[31] S. Komaba, N. Kumagai, Y. Kataoka, *Electrochim Acta*, **47**, 1229-1239 (2002).
[32] I.H. Cho, S.S. Kim, S.C. Shin, N.S. Choi, *Electrochem Solid St*, **13**, A168-A172 (2010).
[33] Y. Hiramatsu, Y. Oka, *International Journal of Rock Mechanics and Mining Sciences & Geomechanics Abstracts*, **3**, 89-90 (1966).
[34] G.M. Hu, H. Otaki, M. Lin, *Miner Eng*, **14**, 1199-1211 (2001).
[35] D. Golchert, R. Moreno, M. Ghadiri, J. Litster, *Powder Technology*, **143–144**, 84-96 (2004).

초록

리튬이온전지는 현재 모바일 전자기기들과 전기자동차의 동력원으로 널리 사용되고 있다. 이 때에 리튬이온전지가 충족해야 할 다양한 요구조건이 있으며 그 중 하나가 바로 높은 부피당 에너지 밀도이다. 부피당 에너지 밀도는 전극 제작 과정 중 프레싱으로 증가시킬 수 있지만 프레싱 시 가해지는 강한 압력은 전극 활물질을 손상시킬 수 있으며 이러한 입자 손상 현상은 리튬이온전지의 성능에 악영향을 미칠 수 있다.

이 연구에서는 프레싱이 입자 깨짐과 리튬이온전지 성능에 미치는 영향에 대해 알아보았다. 활물질은 스피넬 $LiMn_2O_4$가 사용되었다. FE-SEM, 고온 충방전 및 고온 보관을 통하여 프레싱으로 인해 입자 깨짐이 발생하며 이는 전지 성능을 퇴화시킨 다는 것을 확인하였다.

이러한 문제를 해결하기 위해, 입자 형상와 깨짐 특성 간의 관계를 연구하였다. 우선 입자강도측정기를 이용하여 입자 형상이 깨짐에 미치는 영향을 전극이 아닌 입자의 관점에서 연구하였다. 이 입자강도측정 결과를 해석하기 위한 기준을 hard carbon을 이용하여 정립한 뒤, 이를 $LiMn_2O_4$에 적용하였다. 그 결과, 구형의 $LiMn_2O_4$가 비구형에 비해 깨짐에 대한 저항성이 더 큰 것으로 나타났다.

이렇게 입자의 측면에서 형상과 깨짐에 대한 연구를 바탕으로 전극 차원의 실험을 진행하였다. 각각 구형의 $LiMn_2O_4$와 비구형의 $LiMn_2O_4$로 만들어진 전극을 FE-SEM과 고온 보관 실험을 통해 비교하였다. 그 결과, 구형의 $LiMn_2O_4$로 만들어진 전극이 프레싱 과정에서 깨지는 정도가 적었으며 전극 성능의 측면에서도 유리했다. 이는 입자의 관점에서 진행한 실험과 일관된 결과였다.

본 연구에서는 프레싱 과정에서의 입자 깨짐이 $LiMn_2O_4$를 사용하는 리튬이차전지에서 중요한 요소로 생각해야 한다는 점을 밝혔으며 입자 형상을 조절하는 것을 이에 대한 방안으로 제시하였다. 또한 이러한 입자 깨짐의 문제에 있어서 적절한 기준이 전제된 입자강도측정이 전극 활물질의 기계적 특성을 파악할 수 있는 유용한 도구가 될 수 있다는 점을 시사하였다. 본 연구에서 쓰인 방법들과 이로부터 나온 실험 결과는 $LiMn_2O_4$를 포함한 다양한 활물질에 적용됨으로써 리튬이온전지의 성능을 향상시키는 데에 도움이 될 것이라 예상된다.

.....

주요어 : 리튬이온전지, 프레싱, 깨짐, 형상, $LiMn_2O_4$

학번 2013-22526